

The dynamics of starvation and recovery

1 **Justin D. Yeakel * †‡§, Christopher P. Kempes †‡, and Sidney Redner †¶‡**

2 *School of Natural Science, University of California Merced, Merced, CA, †The Santa Fe Institute, Santa Fe, NM, ¶Department of Physics, Boston University, Boston
3 MA, ‡Contributed equally, and §To whom correspondence should be addressed: jdyeakel@gmail.com

4 5 Submitted to Proceedings of the National Academy of Sciences of the United States of America

6 **The eco-evolutionary dynamics of species are fundamentally linked to the energetic constraints of its constituent individuals.**
7 **Of particular importance are the tradeoffs between reproduction and the dynamics of starvation and recovery in resource-limited environments. To elucidate the consequences of this tradeoff,**
8 **we introduce a minimal nutritional state-structured model that incorporates two classes of consumer: nutritionally replete consumers that reproduce, and undernourished, non-reproducing consumers that are susceptible to mortality. As a function of the transition rates between these two states that are determined by the abundance of resources, the consumer populations can either undergo cyclic dynamics or reach a steady state. We obtain strong constraints on starvation and recovery rates by deriving allometric scaling relationships between body size and a variety of traits and find that population dynamics subject to these constraints are typically driven to a steady state. Moreover, we find that these rates fall within a ‘refuge’ in parameter space, where the probability of extinction of the consumer population is minimized. Thus we identify a potential mechanism that may both drive and constrain the dynamics of animal populations. Our model provides a natural framework that predicts maximum body size for mammals by determining the relative stability of an otherwise homogeneous population to a mutant population with altered percentage of body fat. For body masses $< 1.748 \times 10^7$ g, individuals with increased energetic reserves can invade resident populations, and vice versa for body mass $> 1.748 \times 10^7$ g, thus providing a principled mechanism for a within-lineage driver of Cope’s rule.**

34 foraging | starvation | reproduction

35 **Significance Statement** Energetic investment in somatic maintenance and growth vs. reproduction directly impacts the dynamics of populations among species. Here, we construct a Nutritional State-structured Model (NSM) to assess the population-level effects of starvation and recovery of a consumer population in a resource-limited environment, and use allometric scaling relationships for mammals to establish all timescales and rates. Our model: i. reveals that mammalian energetic rates minimize the probability of stochastic extinction, ii. establishes dynamic bounds on mammalian body size while providing independent theoretical support for the energy equivalence hypothesis, and iii. provides a mechanistic driver for the evolutionary trend towards larger body size known as Cope’s rule.

47 Introduction

48 The behavioral ecology of all organisms is influenced by the energetic state of individuals, which directly influences how they invest reserves in uncertain environments. Such behaviors are generally manifested as tradeoffs between investing in somatic maintenance and growth, or allocating energy towards reproduction (1–3). The timing of these behaviors responds to selective pressure, as the choice of the investment impacts future fitness (4–6). The influence of resource limitation on an organism’s ability to maintain its nutritional stores may lead to repeated delays or shifts in reproduction over the course of an organism’s life.

59 The balance between (a) somatic growth and maintenance, and (b) reproduction depends on resource availability (7). For example, reindeer invest less in calves born after harsh winters (when the mother’s energetic state is depleted) than in calves born after moderate winters (8). Many bird species invest dif-

64 ferently in broods during periods of resource scarcity compared to normal periods (9, 10), sometimes delaying or even foregoing reproduction for a breeding season (1, 11, 12). Even freshwater and marine zooplankton have been observed to avoid reproduction under nutritional stress (13), and those that do reproduce have lower survival rates (2). Organisms may also separate maintenance and growth from reproduction over space and time: many salmonids, birds, and some mammals return to migratory breeding grounds to reproduce after one or multiple seasons in resource-rich environments where they accumulate nutritional reserves (14–16).

75 Physiology also plays an important role in regulating reproductive expenditures during periods of resource limitation. The data collected thus far has shown that diverse mammals (47 species in 10 families) exhibit delayed implantation, whereby females postpone fetal development (blastocyst implantation) until nutritional reserves can be accumulated (17, 18). Many other species (including humans) suffer irregular menstrual cycles and higher abortion rates during periods of nutritional stress (19, 20). In the extreme case of unicellular organisms, nutrition is unavoidably linked to reproduction because the nutritional state of the cell regulates all aspects of the cell cycle (21). The existence of so many independently evolved mechanisms across such a diverse suite of organisms highlights the importance and universality of the fundamental tradeoff between somatic and reproductive investment. However the general dynamic implications of these constraints are unknown.

76 Though straightforward conceptually, incorporating the energetic dynamics of individuals (22) into a population-level framework (22, 23) presents numerous mathematical obstacles (24). An alternative approach involves modeling the macroscale relations that guide somatic versus reproductive investment in a consumer-resource system. For example, macroscale Lotka-Volterra models assume that the growth rate of the consumer population depends on resource density, thus implicitly incorporating the requirement of resource availability for reproduction (25).

101 In this work, we adopt an alternative approach in which we explicitly account for resource limitation and the subsequent effects of starvation. Namely, only individuals with sufficient energetic reserves can reproduce. Such a constraint leads to reproductive time lags due to some members of the population going hungry and then recovering. Additionally, we incorporate the idea that reproduction is strongly constrained allometrically (3), and is not generally linearly related to resource density. As

Reserved for Publication Footnotes

¹⁰⁹ we shall show, these constraints influence the ensuing popula-
¹¹⁰ tion dynamics in dramatic ways.

¹¹¹ ¹¹² Nutritional state-structured model (NSM)

¹¹³ We begin by defining a minimal Nutritional State-structured
¹¹⁴ population Model (NSM), where the consumer population is
¹¹⁵ partitioned into two states: (a) an energetically replete (full)
¹¹⁶ state F , where the consumer reproduces at a constant rate λ
¹¹⁷ and does not die from starvation, and (b) an energetically defi-
¹¹⁸ cient (hungry) state H , where the consumer does not reproduce
¹¹⁹ but dies by starvation at rate μ . The underlying resource R
¹²⁰ evolves by logistic growth with an intrinsic growth rate α and
¹²¹ a carrying capacity C . The rate at which consumers transition
¹²² between states and consume resources is dependent on their
¹²³ overall abundance, the abundance of resources, the efficiency of
¹²⁴ converting resources into metabolism, and how that metabolism
¹²⁵ is partitioned between maintenance and growth purposes. In
¹²⁶ the supplementary information (SI) we provide a fully mechani-
¹²⁷ stic model for each of these dynamics and constants, and show
¹²⁸ that the system produces a simple non-dimensional form which
¹²⁹ we describe below.

¹³⁰ Consumers transition from the full state F to the hungry
¹³¹ state H at a rate σ —the starvation rate—and also in propor-
¹³² tion to the absence of resources ($1 - R$). Conversely, consumers
¹³³ recover from state H to state F at rate $\xi\rho$ and in proportion to
¹³⁴ R , where ξ represents a ratio between maximal resource con-
¹³⁵ sumption and the carrying capacity of the resource. Resources
¹³⁶ are eaten by the hungry consumers at rate $\rho R + \delta$, that accounts
¹³⁷ for their somatic growth (ρR) and maintenance (δ). Full con-
¹³⁸ sumers eat resources at a constant rate β that accounts for max-
¹³⁹ imal maintenance and somatic growth (see SI for mechanistic
¹⁴⁰ derivations of these rates from resource energetics). The NSM
¹⁴¹ represents an ecologically motivated fundamental extension of
¹⁴² the idealized starving random walk model of foraging, which
¹⁴³ focuses on resource depletion, to include reproduction and re-
¹⁴⁴ source replenishment (26–28), and is a more general formulation
¹⁴⁵ than previous models incorporating starvation (29).

In the mean-field approximation, in which the consumers and resources are perfectly mixed, their densities evolve according to the rate equations

$$\begin{aligned}\frac{dF}{dt} &= \lambda F + \xi\rho RH - \sigma(1 - R)F, \\ \frac{dH}{dt} &= \sigma(1 - R)F - \xi\rho RH - \mu H, \\ \frac{dR}{dt} &= \alpha(1 - R)R - (\rho R + \delta)H - \beta F\end{aligned}$$

¹⁴⁶ This system of nondimensional equations follows from a set of first-principle relationships for resource consumption and growth (see SI for a full derivation and the dimensional form). Notice that the total consumer density $F + H$ evolves according to $\frac{dF}{dt} + \frac{dH}{dt} = \lambda F - \mu H$. This resembles the equation of motion for the predator density in the classic Lotka-Volterra model (30), except that the resource density does not appear in the growth term. As discussed above, the attributes of reproduction and mortality have been explicitly apportioned to the full and hungry consumers, respectively, so that the growth in the total density is decoupled from the resource density.

Equation [1] has three fixed points: two trivial fixed points at $(F^*, H^*, R^*) = (0, 0, 0)$ and $(0, 0, 1)$, and one non-trivial,

internal fixed point at

$$\begin{aligned}F^* &= (\sigma - \lambda) \frac{\alpha\lambda\mu^2(\mu + \xi\rho)}{A(\lambda\rho B + \mu\sigma(\beta\mu + \lambda(\delta + \rho)))}, \\ H^* &= (\sigma - \lambda) \frac{\alpha\lambda^2\mu(\mu + \xi\rho)}{A(\lambda\rho B + \mu\sigma(\beta\mu + \lambda(\delta + \rho)))}, \\ R^* &= (\sigma - \lambda) \frac{\mu}{A}.\end{aligned}\quad [2]$$

¹⁵⁷ where $A = (\lambda\xi\rho + \mu\sigma)$ and $B = (\beta\mu\xi + \delta\lambda\xi - \lambda\mu)$. The stability of this fixed point is determined by the Jacobian matrix \mathbf{J} , where each matrix element $J_{ij} = \partial\dot{X}_i/\partial X_j$ when evaluated at the internal fixed point, and \mathbf{X} is the vector (F, H, R) . The parameters in Eq. [1] are such that the real part of the largest eigenvalue of \mathbf{J} is negative, so that the system is stable with respect to small perturbations from the fixed point. Because this fixed point is unique, it is the global attractor for all population trajectories for any initial condition where the resource and consumer densities are both nonzero.

¹⁶⁷ From Eq. [2], an obvious constraint on the NSM is that the reproduction rate λ must be less than the starvation rate σ , so that the consumer and resource densities are positive. The condition $\sigma = \lambda$ thus represents a transcritical (TC) bifurcation (31) that demarcates a physical from an unphysical regime where all steady-state densities become negative after intersecting the trivial fixed point $(F^*, H^*, R^*) = (0, 0, 0)$. The biological implication of the constraint $\lambda < \sigma$ has a simple interpretation—the rate at which a macroscopic organism loses mass due to lack of resources is generally much faster than the rate of reproduction. As we will discuss below, this inequality is a natural consequence of allometric constraints (3) for organisms within empirically observed body size ranges.

¹⁸⁰ In the physical regime of $\lambda < \sigma$, the fixed point [2] may either be a stable node or a limit cycle (Fig. 1). In continuous-time systems, a limit cycle arises when a pair of complex conjugate eigenvalues crosses the imaginary axis to attain positive real parts (32). This Hopf bifurcation is defined by $\text{Det}(\mathbf{S}) = 0$, with \mathbf{S} the Sylvester matrix, which is composed of the coefficients of the characteristic polynomial of the Jacobian matrix (33). As the system parameters are tuned to be within the stable regime, but close to the Hopf bifurcation, the amplitude of the transient cycles becomes large. Given that ecological systems are constantly being perturbed (34), the onset of transient cycles, even though they decay with time in the mean-field description, can increase the extinction risk (35–37).

¹⁹³ When the starvation rate $\sigma \gg \lambda$, a substantial fraction of the consumers are driven to the hungry non-reproducing state. Because reproduction is inhibited, there is a low steady-state consumer density and a high steady-state resource density. However, if $\sigma/\lambda \rightarrow 1$ from above, the population is overloaded with energetically-replete (reproducing) individuals, thereby promoting transient oscillations between the consumer and resource densities (Fig. 1). If the starvation rate is low enough that the Hopf bifurcation is crossed, these oscillations become stable over time. This threshold occurs at higher values of the starvation rate as the recovery rate ρ increases, such that the range of parameter space giving rise to cyclic dynamics also increases with higher recovery rates.

²⁰⁷ Role of allometry

²⁰⁸ While there are no a priori constraints on the parameters in the NSM, most organisms correspond to restricted portions of the parameter space. Here we use allometric scaling relations to constrain the covariation of rates in a principled and biologically meaningful manner. Allometric scaling relations highlight

215 derived from a small set of assumptions and below we describe 271 an adjusted starting mass of $m'_0 = \epsilon_\sigma \epsilon_\lambda M$, in which case
 216 our framework to determine the covariation of timescales and
 217 rates across the range of mammals for each of the key param-
 218 ters of our model (cf. ref. 38). We are thereby able to define the
 219 regime of dynamics occupied by the entire class of mammals,
 220 along with the key differences between the largest and smallest
 221 mammals.

222 Nearly all of the rates described in the NSM are determined
 223 by consumer metabolism, which can be used to describe a vari-
 224 ety of organismal features (39). The scaling relation between an

225 organism's metabolic rate B and its body mass M at reproduc-
 226 tive maturity is known to scale as $B = B_0 M^\eta$ (40), where the
 227 scaling exponent η is typically close to 2/3 or 3/4 for metazoans
 228 (e.g., ref. 39), and has taxonomic shifts for unicellular species
 229 between $\eta \approx 1$ in eukaryotes and $\eta \approx 1.76$ in bacteria (3, 41).

230 Several efforts have shown how a partitioning of B be-
 231 tween growth and maintenance purposes can be used to derive
 232 a general equation for both the growth trajectories and growth
 233 rates of organisms ranging from bacteria to metazoans (3, 42–
 234 45). This relation is derived from the simple balance condition
 235 (3, 42–45)

$$B_0 m^\eta = E_m \frac{dm}{dt} + B_m m,$$

[3]

$$\frac{dm}{dt} E'_m = -B_m m$$

[7]

236 where E_m is the energy needed to synthesize a unit of mass, B_m
 237 is the metabolic rate to support an existing unit of mass, and
 238 m is the mass of the organism at any point in its development.
 239 This balance has the general solution (3, 46)

$$\left(\frac{m(t)}{M}\right)^{1-\eta} = 1 - \left[1 - \left(\frac{m_0}{M}\right)^{1-\eta}\right] e^{-a(1-\eta)t/M^{1-\eta}},$$

[4]

240 where, for $\eta < 1$, $M = (B_0/B_m)^{1/(1-\eta)}$ is the asymptotic mass,
 241 $a = B_0/E_m$, and m_0 is mass at birth, itself varying allometri-
 242 cally (see SI). We now use this solution to define the timescale
 243 for reproduction and recovery from starvation (Fig. 2; see (43)
 244 for a detailed presentation of these timescales). The time that
 245 it takes to reach a particular mass ϵM is given by the timescale

$$\tau(\epsilon) = \ln \left[\frac{1 - (m_0/M)^{1-\eta}}{1 - \epsilon^{1-\eta}} \right] \frac{M^{1-\eta}}{a(1-\eta)},$$

[5]

246 where we will define values of ϵ to describe a set of rates within
 247 our model. For the time to reproduce, $t_\lambda = \tau(\epsilon_\lambda)$, where ϵ_λ
 248 is the fraction of the asymptotic mass where an organism is
 249 reproductively mature and should be close to one (typically
 250 $\epsilon_\lambda \approx 0.95$; 42). The growth rate is then given by $\lambda = \ln(v)/t_\lambda$
 251 where v is the number of offspring produced, and for any con-
 252 stant value of ϵ_λ , this rate will scale as $\lambda \propto M^{\eta-1}$ for $M \gg m_0$
 253 (3, 42–45).

254 The rate of recovery $\rho = 1/t_\rho$ requires that an organism
 255 accrues sufficient tissue to transition from the hungry to the
 256 full state. Since only certain tissues can be digested for energy
 257 (for example the brain cannot be degraded to fuel metabolism),

258 we define the rates for starvation, death, and recovery by the

259 timescales required to reach, or return from, specific fractions

260 of the replete-state mass (Fig. 3; see SI, Table I for parameter-
 261 izations). We define $m_\sigma = \epsilon_\sigma M$, where $\epsilon_\sigma < 1$ is the fraction
 262 of replete-state mass where reproduction ceases. This fraction
 263 will deviate from a constant if tissue composition systematically
 264 scales with adult mass. For example, making use of the obser-
 265 vation that body fat in mammals scales with overall body size
 266 according to $M_{\text{fat}} = f_0 M^\gamma$ and assuming that once this mass
 267 is fully digested the organism starves, this would imply that
 268 $\epsilon_\sigma = 1 - f_0 M^\gamma / M$. It follows that the recovery timescale,
 269 the time to go from $m = \epsilon_\sigma \epsilon_\lambda M$ to $m = \epsilon_\lambda M$ (Fig. 2). Using
 270 Eqs. [4] and [5] this timescale is given by simply considering

$$t_\rho = \ln \left[\frac{1 - (\epsilon_\sigma \epsilon_\lambda)^{1-\eta}}{1 - \epsilon_\lambda^{1-\eta}} \right] \frac{M^{1-\eta}}{a'(1-\eta)}$$

[6]

271 where $a' = B_0/E'_m$ accounts for possible deviations in the
 272 biosynthetic energetics during recovery (see SI). It should be
 273 noted that more complicated ontogenetic models explicitly han-
 274 dle storage (45), whereas this feature is implicitly covered by
 275 the body fat scaling in our framework.

276 To determine the starvation rate, σ , we are interested in the
 277 time required for an organism to go from a mature adult that
 278 reproduces at rate λ , to a reduced-mass hungry state where re-
 279 production is impossible. For starving individuals we assume
 280 that an organism must meet its maintenance requirements by
 281 using the digestion of existing mass as the sole energy source.
 282 This assumption implies the following simple metabolic balance

$$\frac{dm}{dt} E'_m = -B_m m$$

[7]

284 OR

$$\frac{dm}{dt} = -\frac{a'}{M^{1-\eta}} m$$

[8]

285 where E'_m is the amount of energy stored in a unit of exist-
 286 ing body mass, which differs from E_m , the energy required to
 287 synthesis a unit of biomass (45). Given the replete mass, M ,
 288 of an organism, the above energy balance prescribes the mass
 289 trajectory of a non-consuming organism:

$$m(t) = M e^{-a't/M^{1-\eta}}.$$

[9]

290 The timescale for starvation is given by the time it takes $m(t)$
 291 to reach $\epsilon_\sigma M$, which gives

$$t_\sigma = -\frac{M^{1-\eta}}{a'} \ln(\epsilon_\sigma).$$

[10]

292 The starvation rate is then $\sigma = 1/t_\sigma$, which scales with replete-
 293 state mass as $1/M^{1-\eta} \ln(1 - f_0 M^\gamma / M)$. An important feature
 294 is that σ does not have a simple scaling dependence on λ (Fig.
 295 3), which is important for the dynamics that we later discuss.

296 The time to death should follow a similar relation, but de-
 297 fined by a lower fraction of replete-state mass, $m_\mu = \epsilon_\mu M$ where
 298 $\epsilon_\mu < \epsilon_\sigma$. Suppose, for example, that an organism dies once it
 299 has digested all fat and muscle tissues, and that muscle tissue
 300 scales with body mass according to $M_{\text{musc}} = u_0 M^\zeta$. This gives
 301 $\epsilon_\mu = 1 - (f_0 M^\gamma + u_0 M^\zeta) / M$. Muscle mass has been shown
 302 to be roughly proportional to body mass (47) in mammals and
 303 thus ϵ_μ is merely ϵ_σ minus a constant. The time to go from
 304 starvation to death is the total time to reach $\epsilon_\mu M$ minus the
 305 time to starve, or

$$t_\mu = -\frac{M^{1-\eta}}{a'} \ln(\epsilon_\mu) - t_\sigma,$$

[11]

297 Although the rate equations [1] are general, here we focus
 298 on parameterizations for terrestrial-bound endotherms, specif-
 299 ically mammals, which range from a minimum of $M \approx 1\text{g}$
 300 to a maximum of $M \approx 10^7\text{g}$ (the early Oligocene Indricotheriinae and the Miocene
 301 Deinotheriinae). Investigating other classes of organisms would
 302 simply involve altering the metabolic exponents and scalings
 303 associate with ϵ . Moreover, we emphasize that our allometric
 304 is fully digested the organism starves, this would imply that
 305 equations describe mean relationships, and do not account for
 306 the variance associated with individual species.

319 Stabilizing effects of allometric constraints

320 As the allometric derivations of the NSM rate laws reveal, star-
321 vation and recovery rates are not independent parameters, and
322 the biologically relevant portion of the phase space shown in
323 Fig. 1 is constrained via covarying parameters. Given the pa-
324 rameters of terrestrial endotherms, we find that the starvation
325 rate σ and the recovery rate ρ are constrained to lie within a
326 small region of potential values (Fig. 4) for the known range
327 of body sizes M . We thus find that the dynamics for all mam-
328 malian body sizes are confined to the steady-state regime of the
329 NSM and that limit-cycle behavior is precluded. Incorporating
330 uncertainty in allometric parameters (20% variation around the
331 mean; Fig. 4), we find that, for larger M , the distance to the TC
332 and Hopf bifurcation decreases. These results suggest that small
333 mammals are marginally less prone to population oscillations—
334 both stable limit cycles and transient cycles—than mammals
335 with larger body size. However, starvation and recovery rates
336 across all values of M fall squarely in the steady state region at
337 some distance from the Hopf bifurcation. This result suggests
338 that cyclic population dynamics should be rare, particularly in
339 environments where resources are limiting.

340 Previous studies used allometric constraints to explain the
341 periodicity of cyclic populations (48–50), suggesting a period
342 $\propto M^{0.25}$. However this relation seems to hold only for some
343 species (51), and potential drivers of variation and systemati-
344 cally different behavior range from predator and/or prey lifes-
345 pans to competitive dynamics (52, 53). Statistically significant
346 support for the existence of population cycles among mammals
347 is relatively rare, though predominantly based on time series
348 for small mammals (54). However the longer gestational times
349 and increased difficulty in collecting adequate data precludes
350 obtaining similar-quality information for larger organisms.

351 Extinction risk

352 Within our model, higher rates of starvation result in a larger
353 flux of the population to the hungry state. In this state, re-
354 production is absent, thus increasing the likelihood of extinc-
355 tion. From the perspective of population survival, it is the rate
356 of starvation relative to the rate of recovery that determines
357 the long-term dynamics of the various species (Fig. 1). We
358 therefore examine the competing effects of cyclic dynamics vs.
359

360 changes in steady-state density on extinction risk, both as func-
361 tions of σ and ρ . To this end, we computed the probability of ex-
362 tinction, where we define extinction as a population trajectory
363 falling below one fifth of the allometrically constrained steady
364 state at any time between $t = 10^8$ and $t = 10^{10}$. This proce-
365 dure is repeated for 50 replicates of the continuous-time system
366 shown in Eq. 1 for organisms with mass ranging from 10^2 to 10^6
367 grams. In each replicate the initial densities are chosen to be
368 (XF^* , XH^* , R^*), with X a random variable that is uniformly
369 distributed in [0, 2]. By allowing the rate of starvation to vary,
370 we assessed extinction risk across a range of values for σ and ρ
371 between ca. 10^{-7} to 10^{-3} . As expected, higher rates of extinc-
372 tion correlate with both high values of σ if ρ is small, and high
373 values of ρ if σ is small. For low values of σ and high values
374 of ρ , the increased extinction risk results from transient cycles
375 with larger amplitudes as the system nears the Hopf bifurcation
376 (Fig. 5). For high values of σ and low values of ρ , increased
377 extinction risk arises because of the decrease in the steady-state
378 consumer population density (Figs. 1B, 5). This interplay cre-
379 ates an ‘extinction refuge’, such that for a constrained range of
380 σ and ρ , extinction probabilities are minimized.

381 We find that the allometrically constrained values of σ and
382 ρ fall squarely within the extinction refuge across a range of
383 M (Fig. 5A–C, white points). These values are close enough
384 to the Hopf bifurcation to avoid low steady-state densities, and
385 far enough away to avoid large-amplitude transient cycles. The

386 feature that allometric values of σ and ρ fall within this rel-
387 atively small window supports the possibility that a selective
388 mechanism has constrained the physiological conditions that
389 drive starvation and recovery rates within populations. Such a
390 mechanism would select for organism physiology that generates
391 appropriate σ and ρ values that serve to minimize extinction
392 risk. This selection could occur via the tuning of body fat per-
393 centages, metabolic rates, and biomass maintenance efficiencies.
394 We also find that as body size increases, the amount of low ex-
395 tinction risk parameter space becomes smaller (Fig. 5A–C),
396 suggesting that the population dynamics of larger organisms
397 are more sensitive to smaller changes in physiological rates con-
398 sequent to the TC trolling starvation and recovery. *To summarize, our finding*
399 *that the allometrically-determined parameters fall within this*
400 *low extinction probability region suggests that the NSM dynam-*
401 *ics may both drive—and constrain—natural animal popula-*
402 *tions.*

403 Dynamic and energetic barriers to body size

404 Metabolite transport constraints are widely thought to place
405 strict boundaries on biological scaling (39, 55, 56) and thereby

406 lead to specific predictions on the minimum possible body size

407 for organisms (57). Above this bound, a number of energetic
408 and evolutionary mechanisms have been explored to assess the
409 costs and benefits associated with larger body masses, partic-
410 ularly for mammals. One important such example is the *fast-*
411 *ing endurance hypothesis*, which contends that larger body size,
412 with consequent lower metabolic rates and increased ability to
413 maintain more endogenous energetic reserves, may buffer or-
414 ganisms against environmental fluctuations in resource avail-
415 ability (58). Over evolutionary time, terrestrial mammalian lin-
416 eages show a significant trend towards larger body size (known
417 as Cope’s rule) (59–62), and it is thought that within-lineage
418 drivers generate selection towards an optimal upper bound of
419 roughly 10^7 grams (59), a value that is likely limited by higher

420 extinction risk for large taxa over longer timescales (60). These
421 trends are thought to be driven by a combination of climate
422 change and niche availability (62); however the underpinning
423 energetic costs and benefits of larger body sizes, and how they
424 influence dynamics over ecological timescales, have not been ex-
425 plored. We argue that the NSM provides a suitable framework
426 to explore these issues.

427 The NSM correctly predicts that species with smaller
428 masses have larger steady-state population densities (Fig. 6A).
429 Moreover, we show that the NSM provides independent the-
430 oretical support for the energy equivalence hypothesis and
431 Damuth’s Law (63–65). The energy equivalence hypothesis ar-
432 gues that the total energy use, B_{tot} , of a population is constant
433 independent of species size (63–65). This hypothesis is based on
434 observations showing that the steady state abundance, N^* , of a
435 species is proportional to the inverse of individual metabolism,
436 such that $N^* \propto M^{-3/4}/B_0$ (64, 65). This relationship im-
437 plies that $B_{\text{tot}} = N^*B(M) = Q$, where Q is a constant, and
438 has been shown to hold in both mammalian and vascular plant
439 communities (63–65). Figure 6A shows that both F^* and H^*
440 scale as $M^{-\eta}$ over a wide range of organism sizes and Figure 6B
441 shows that F^*B is nearly constant over this same range. This
442 result is remarkable because it illustrates that the steady state
443 values of the NSM combined with the derived timescales natu-
444 rally give rise to energy equivalence. Our model shows that the
445 equivalence breaks down at the maximum observed body sizes
446 for mammals, suggesting that this maximum is a hard limit
447 where deviations outside of this range are energetically subop-
448 timal. In the framework of our model, the total metabolic rate
449 of F and H becomes infinite at a finite mass, and occur at the
450 same scale where the steady state resources vanish (Fig. 6).
451 This asymptotic behavior is governed by body sizes at which
452 ϵ_μ and ϵ_λ equal zero causing the timescales to become infinite

(see Equation 11) and the rates μ and λ to equal zero. The NSM predicts organismal mass to increase if $M < M_{\text{opt}}$ and decrease if $M > M_{\text{opt}}$. This value is close to but smaller than the asymptotic upper bound for terrestrial mammal body size predicted by the NSM, however it is remarkably close to the size predicted by the NSM at $M_{\text{max}} = 6.54 \times 10^7$. Moreover, M_{max} , which is entirely independent estimates of the largest land mammals, the early determined by the population-level consequences of energetic constraints, is close to the maximum body size observed in the North American mammalian fossil record (59), as well as the mass predicted from an evolutionary model of body size evolution (60). It should be noted that the asymptotic behavior and provides independent theoretical support for the observational upper bound depend only on the scaling of body composition of a ‘maximum body size attractor’ for North American mammals outlined by Alroy (59). While the state of the environment, as well as the competitive landscape, will determine whether specific body sizes are selected for or against (62), we propose that the dynamics of starvation and recovery described in the NSM provide a general within-lineage mechanism for the evolution of larger body size among terrestrial mammals.

We contend that the NSM provides a mechanistic understanding of the energetic dynamics that give rise to both observed limitations on mammalian body size, as well as the observed trend towards larger body size over evolutionary time. The NSM predicts that the steady state resource density R^* decreases with increasing body size of the consumer population (Fig. 6C), and classic resource competition theory predicts that the species surviving on the lowest resource abundance will outcompete others (67–69). Thus, the combined NSM steady-state dynamics and allometric timescales predict that larger mammals have an intrinsic competitive advantage given a common resource, but does not offer a within-lineage mechanism by which larger body sizes are selected for.

To examine whether the NSM could provide such a mechanism, we begin by noting that a theoretical upper bound on mammalian body size is given by $\epsilon_\sigma = 0$, where mammals are entirely composed of metabolic reserves, and this occurs at $M = 8.3 \times 10^8$, or 120 times the mass of a male African elephant. Next we examine to what extent a more realistic upper bound to body mass may serve as an evolutionary attractor, thus providing a suitable within-lineage mechanism for Cope’s rule. We directly assess the susceptibility of an otherwise homogeneous population to invasion by a mutated subset of the population (denoted by $'$) where individuals have a modified proportion of body fat $M' = M(1+\chi)$. For the allowable values of χ the adjusted mass should exceed the amount of body fat, $1+\chi > \epsilon_\sigma$, and the adjusted time to reproduce must be positive, which given Equation 5, implies that $1 - \epsilon_\lambda^{1-\eta} (1+\chi)^{1-\eta} > 0$.

Together these conditions imply that $\chi \in (-f_0 M^{\gamma-1}, 1/\epsilon_\lambda - 1)$ where the upper bound approximately equals 0.05. The modified mass adjusts our model via the altered rates of starvation $\sigma(M')$, recovery $\rho(M')$, and the maintenance of both starved $\delta(M')$ and full consumers $\beta(M')$. Importantly, ϵ_σ , which determines the point along the growth curve that defines the body composition of starved foragers, is assumed to remain unchanged for the invader population (see SI for detailed derivations of invader rates).

To assess the susceptibility of the resident population to invasion, we determine which consumer has a lower steady-state resource density for a given value of χ , again with the expectation that populations able to survive on lower resource densities have a competitive advantage (67). We find that for $M \leq 1.748 \times 10^7$ g, having additional body fat ($\chi > 0$) results in a lower steady state resource density ($R'^* < R^*$), such that the invader has an intrinsic competitive advantage over the resident population. However, for $M > 1.748 \times 10^7$ g, leaner individuals ($\chi < 0$) have lower resource steady state densities, switching the advantage for higher values of M .

The observed switch in susceptibility as a function of χ at $M_{\text{opt}} = 1.748 \times 10^7$ g thus serves as an attractor, such that

References

1. Martin TE (1987) Food as a limit on breeding birds: A life-history perspective. *Annu. Rev. Ecol. Syst.* 18:453–487.
2. Kirk KL (1997) Life-history responses to variable environments: Starvation and reproduction in planktonic rotifers. *Ecology* 78:434–441.
3. Kempes CP, Dutkiewicz S, Follows MJ (2012) Growth, metabolic partitioning, and the size of microorganisms. *Proc. Natl. Acad. Sci. USA* 109:495–500.
4. Mangel M, Clark CW (1988) *Dynamic Modeling in Behavioral Ecology* (Princeton University Press, Princeton).
5. Mangel M (2014) Stochastic dynamic programming illuminates the link between environment, physiology, and evolution. *B. Math. Biol.* 77:857–877.
6. Yeakel JD, Dominy NJ, Koch PL, Mangel M (2014) Functional morphology, stable isotopes, and human evolution: a model of consilience. *Evolution* 68:190–203.
7. Morris DW (1987) Optimal allocation of parental investment. *Oikos* 49:332–339.
8. Tveraa T, Fauchald P, Henaug C, Yoccoz NG (2003) An examination of a compensatory relationship between food limitation and predation in semi-domestic reindeer. *Oecologia* 137:370–376.
9. Daan S, Dijkstra C, Drent R, Meijer T (1989) in *Acta XIX Congressus Internationalis Ornithologici, Volume I: Proceedings XIX International Ornithological Congress, 1986, Ottawa*, ed Ouellet H (Proceedings XIX International Ornithological Congress, Ottawa), pp 392–407.

- 584 10. Jacot A, Valcu M, van Oers K, Kempenaers B (2009) Experimental nest site limitation affects reproductive strategies and parental investment in a hole-nesting passerine. *Animal Behaviour* 77:1075–1083.
- 585 11. Stearns SC (1989) Trade-offs in life-history evolution. *Funct. Ecol.* 3:259.
- 586 12. Barboza P, Jorde D (2002) Intermittent fasting during winter and spring affects body composition and reproduction of a migratory duck. *J Comp Physiol B* 172:419–434.
- 587 13. Threlkeld ST (1976) Starvation and the size structure of zooplankton communities. *Freshwater Biol.* 6:489–496.
- 588 14. Weber TP, Ens BJ, Houston AI (1998) Optimal avian migration: A dynamic model of fuel stores and site use. *Evolutionary Ecology* 12:377–401.
- 589 15. Mduma SAR, Sinclair ARE, Hilborn R (1999) Food regulates the Serengeti wildebeest: a 40-year record. *J. Anim. Ecol.* 68:1101–1122.
- 590 16. Moore JW, Yeakel JD, Peard D, Lough J, Beere M (2014) Life-history diversity and its importance to population stability and persistence of a migratory fish: steelhead in two large North American watersheds. *J. Anim. Ecol.* 83:1035–1046.
- 591 17. Mead RA (1989) in *Carnivore Behavior, Ecology, and Evolution*, ed Gittleman JL (Springer US, Ithaca), pp 437–464.
- 592 18. Sandell M (1990) The evolution of seasonal delayed implantation. *Q Rev Biol* 65:23–42.
- 593 19. Bulik CM, et al. (1999) Fertility and reproduction in women with anorexia nervosa. *J. Clin. Psychiatr.* 60:130–135.
- 594 20. Trites AW, Donnelly CP (2003) The decline of Steller sea lions *Eumetopias jubatus* in Alaska: a review of the nutritional stress hypothesis. *Mammal Rev.* 33:3–28.
- 595 21. Glazier DS (2009) Metabolic level and size scaling of rates of respiration and growth in unicellular organisms. *Funct. Ecol.* 23:963–968.
- 596 22. Kooijman SALM (2000) *Dynamic Energy and Mass Budgets in Biological Systems* (Cambridge).
- 597 23. Sousa T, Domingos T, Poggiale JC, Kooijman SALM (2010) Dynamic energy budget theory restores coherence in biology. *Philos. T. Roy. Soc. B* 365:3413–3428.
- 598 24. Diekmann O, Metz JA (2010) How to lift a model for individual behaviour to the population level? *Philos. T. Roy. Soc. B* 365:3523–3530.
- 599 25. Murdoch WW, Briggs CJ, Nisbet RM (2003) *Consumer-resource Dynamics*, Monographs in population biology (Princeton University Press, Princeton) Vol. 36.
- 600 26. Benichou O, Redner S (2014) Depletion-Controlled Starvation of a Diffusing Forager. *arXiv* pp 1–5.
- 601 27. Bénichou O, Chupeau M, Redner S (2016) Role of depletion on the dynamics of a diffusing forager. *Journal of Physics A:*
- 602 28. Chupeau M, Bénichou O, Redner S (2016) Universality classes of foraging with resource renewal. *Phys. Rev. E* 93:032403.
- 603 29. Persson L, Leonardsson K, De Roos AM, Gyllenberg M, Christensen B (1998) Ontogenetic scaling of foraging rates and the dynamics of a size-structured consumer-resource model. *Theor Popul Biol* 54:270–293.
- 604 30. Murray JD (2011) *Mathematical Biology: I. An Introduction*, Interdisciplinary Applied Mathematics (Springer New York) Vol. 110.
- 605 31. Strogatz SH (2008) *Nonlinear Dynamics and Chaos: With Applications to Physics, Biology, Chemistry, and Engineering*, Studies in nonlinearity (Westview Press, Boulder).
- 606 32. Guckenheimer J, Holmes P (1983) *Nonlinear Oscillations, Dynamical Systems, and Bifurcations of Vector Fields* (Springer, New York).
- 607 33. Gross T, Feudel U (2004) Analytical search for bifurcation surfaces in parameter space. *Physica D* 195:292–302.
- 608 34. Hastings A (2001) Transient dynamics and persistence of ecological systems. *Ecol. Lett.* 4:215–220.
- 609 35. Neubert M, Caswell H (1997) Alternatives to resilience for measuring the responses of ecological systems to perturbations. *Ecology* 78:653–665.
- 610 36. Caswell H, Neubert MG (2005) Reactivity and transient dynamics of discrete-time ecological systems. *J Differ Equ Appl* 11:295–310.
- 611 37. Neubert M, Caswell H (2009) Detecting reactivity. *Ecology* 90:2683–2688.
- 612 38. Yodzis P, Innes S (1992) Body size and consumer-resource dynamics. *Am. Nat.* 139:1151–1175.
- 613 39. Brown J, Gillooly J, Allen A, Savage V, West G (2004) Toward a metabolic theory of ecology. *Ecology* 85:1771–1789.
- 614 40. West GB, Woodruff WH, Brown JH (2002) Allometric scaling of metabolic rate from molecules and mitochondria to cells and mammals. *Proc. Natl. Acad. Sci. USA* 99 Suppl 1:2473–2478.
- 615 41. DeLong JP, Okie JG, Moses ME, Sibly RM, Brown JH (2010) Shifts in metabolic scaling, production, and efficiency across major evolutionary transitions of life. *Proc. Natl. Acad. Sci. USA* 107:12941–12945.
- 616 42. West GB, Brown JH, Enquist BJ (2001) A general model for ontogenetic growth. *Nature* 413:628–631.
- 617 43. Moses ME, et al. (2008) Revisiting a Model of Ontogenetic Growth: Estimating Model Parameters from Theory and Data. *Am. Nat.* 171:632–645.
- 618 44. Gillooly JF, Charnov EL, West GB, Savage VM, Brown JH (2002) Effects of size and temperature on developmental time. *Nature* 417:70–73.
- 619 45. Hou C, et al. (2008) Energy uptake and allocation during ontogeny. *Science* 322:736–739.
- 620 46. Bettencourt LMA, Lobo J, Helbing D, Kuhnert C, West GB (2007) Growth, innovation, scaling, and the pace of life in cities. *Proc. Natl. Acad. Sci. USA* 104:7301–7306.
- 621 47. Folland JP, Mc Cauley TM, Williams AG (2008) Allometric scaling of strength measurements to body size. *Eur J Appl Physiol* 102:739–745.
- 622 48. Calder III WA (1983) An allometric approach to population cycles of mammals. *J. Theor. Biol.* 100:275–282.
- 623 49. Peterson RO, Page RE, Dodge KM (1984) Wolves, moose, and the allometry of population cycles. *Science* 224:1350–1352.
- 624 50. Krukonis G, Schaffer WM (1991) Population cycles in mammals and birds: Does periodicity scale with body size? *J. Theor. Biol.* 148:469–493.
- 625 51. Hendriks AJ, Mulder C (2012) Delayed logistic and Rosenzweig–MacArthur models with allometric parameter setting estimate population cycles at lower trophic levels well. *Ecol Complex* 9:43–54.
- 626 52. Kendall BE, et al. (1999) Why do populations cycle? A synthesis of statistical and mechanistic modeling approaches. *Ecology* 80:1789–1805.
- 627 53. Höglstedt G, Seldal T, Breistøl A (2005) Period length in cyclic animal populations. *Ecology* 86:373–378.
- 628 54. Kendall, Prendergast, Bjornstad (1998) The macroecology of population dynamics: taxonomic and biogeographic patterns in population cycles. *Ecol. Lett.* 1:160–164.
- 629 55. Brown J, Marquet P, Taper M (1993) Evolution of body size: consequences of an energetic definition of fitness. *Am. Nat.* 142:573–584.
- 630 56. West GB, Brown JH, Enquist BJ (1997) A general model for the origin of allometric scaling laws in biology. *Science* 276:122–126.

- 716 57. West GB, Woodruff WH, Brown JH (2002) Allometric scal- 738
717 ing of metabolic rate from molecules and mitochondria to 739 65. Enquist BJ, Brown JH, West GB (1998) Allometric scaling
718 cells and mammals. *Proc. Natl. Acad. Sci. USA* 99 Suppl 740 of plant energetics and population density. *Nature* 395:163–
719 1:2473–2478. 741
720 58. Millar J, Hickling G (1990) Fasting endurance and the evo- 742 66. Kempes CP, Wang L, Amend JP, Doyle J, Hoehler T (2016)
721 lution of mammalian body size. *Funct. Ecol.* 4:5–12. 743 Evolutionary tradeoffs in cellular composition across diverse
722 59. Alroy J (1998) Cope's rule and the dynamics of body 744 745 bacteria. *ISME J* 10:2145–2157.
723 mass evolution in North American fossil mammals. *Science* 280:731–734. 746
724 60. Clauset A, Redner S (2009) Evolutionary model of species 747 67. Tilman D (1981) Tests of resource competition theory using
725 body mass diversification. *Phys. Rev. Lett.* 102:038103. 748 four species of lake michigan algae. *Ecology* 62:802–815.
726 61. Smith FA, et al. (2010) The evolution of maximum body 749 68. Dutkiewicz S, Follows MJ, Bragg JG (2009) Modeling the
727 size of terrestrial mammals. *Science* 330:1216–1219. 750 coupling of ocean ecology and biogeochemistry. *Global Bio-*
728 62. Saarinen JJ, et al. (2014) Patterns of maximum body 751 69. Barton AD, Dutkiewicz S, Flierl G, Bragg J, Follows MJ
729 size evolution in Cenozoic land mammals: Eco-evolutionary 752 (2010) Patterns of diversity in marine phytoplankton. *Sci-*
730 processes and abiotic forcing. *Proc Biol Sci* 281:20132049. 753
731 63. Damuth J (1987) Interspecific allometry of population den- 754 753 **ACKNOWLEDGMENTS.** We thank Luis Bettencourt, Jean Philippe Gibert,
732 sity in mammals and other animals: the independence of 755 Eric Libby, and Seth Newsome for helpful discussions and comments on the
733 body mass and population energy-use. *Biol. J. Linn. Soc.* 31:193–246. 756 manuscript. J.D.Y. was supported by startup funds at the University of California,
734 757 Merced, and an Omidyar Postdoctoral Fellowship at the Santa Fe Institute. C.P.K.
735 758 was supported by an Omidyar Postdoctoral Fellowship at the Santa Fe Institute.
736 64. Allen AP, Brown JH, Gillooly JF (2002) Global biodi- 759 S.R. was supported by grants DMR-1608211 and 1623243 from the National
737 versity, biochemical kinetics, and the energetic-equivalence 760 Science Foundation, and by the John Templeton Foundation, all at the Santa Fe
738 Institute.

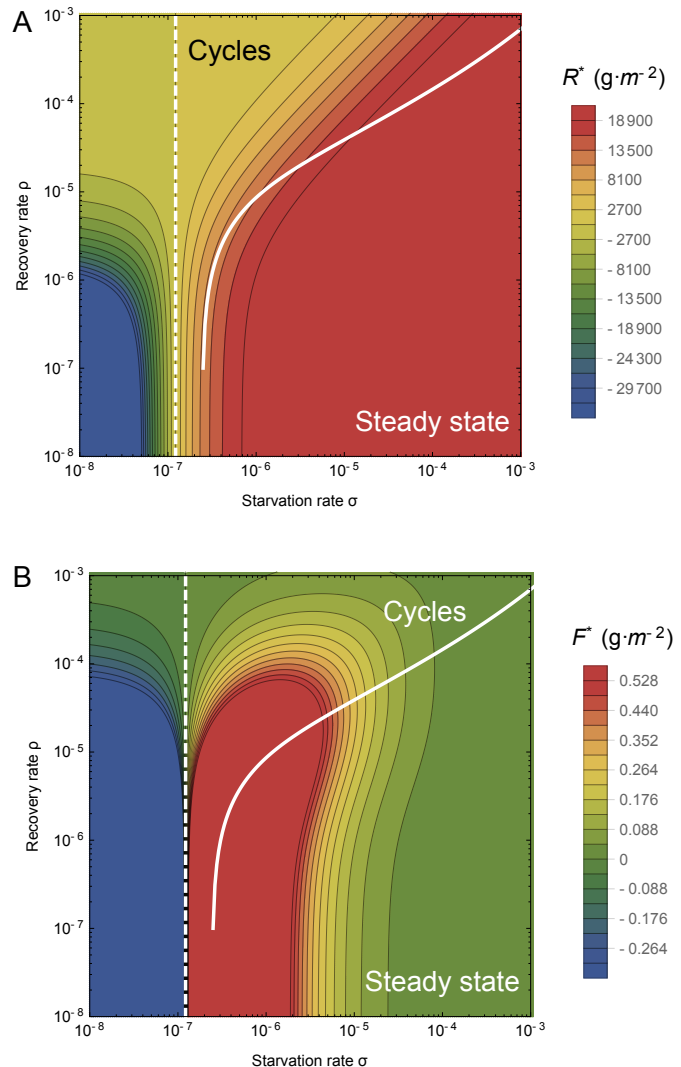


Fig. 1: The transcritical (dashed) and Hopf bifurcation (solid) as a function of the starvation rate σ and recovery rate ρ for a 100g consumer. These bifurcation conditions separate parameter space into unphysical, cyclic, and steady state dynamic regimes. The colors show the steady state densities for (A) the resource R^* and the (B) energetically replete consumers F^* , (warmer colors denote higher densities). Steady state densities for the energetically deficient consumers H^* (not shown) scale with those for F^* .

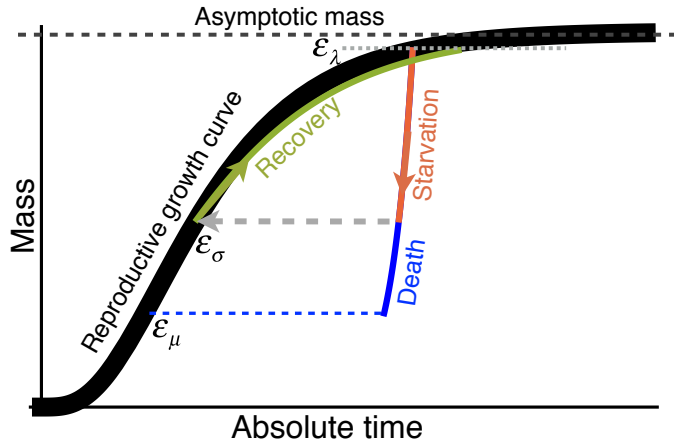


Fig. 2: The growth trajectory over absolute time of an individual organism as a function of body mass. Initial growth follows the black trajectory to an energetically replete reproductive adult mass $m = \epsilon_\lambda M$ which we assume is 95% asymptotic mass M . Starvation follows the red trajectory to $m = \epsilon_\sigma \epsilon_\lambda M$. Recovery follows the green curve to the replete adult mass, where this trajectory differs from the original growth because only fat is being regrown which requires different energetics and a longer time to reach $\epsilon_\lambda M$. Alternatively, death from starvation follows the blue trajectory to $m = \epsilon_\mu \epsilon_\lambda M$.

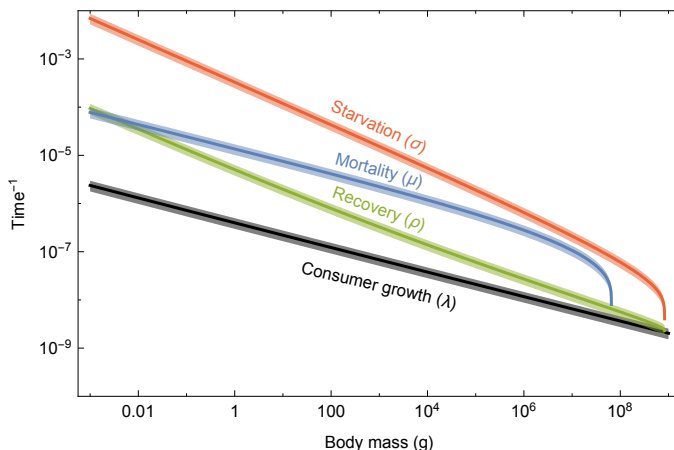


Fig. 3: Allometrically constrained starvation rate $\sigma = 1/t_\sigma$ (red), mortality $\mu = 1/t_\mu$ (blue) and recovery rate $\rho = 1/t_\rho$ (green) relative to the reproductive rate $\lambda = 1/t_\lambda$ (black) as a function of body mass (see Equations 5, 6, 10, and 11). The rate of starvation is greater than the rate of reproduction for all realized terrestrial endotherm body sizes. Mean values $\pm 25\%$ variation are shown by the shaded region for each rate.

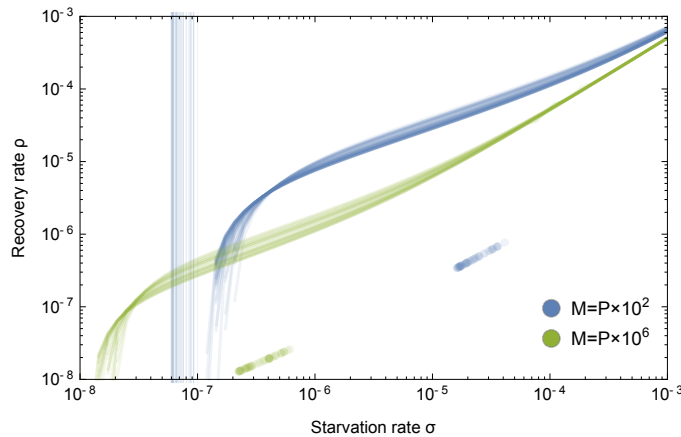


Fig. 4: Transcritical (vertical lines) and Hopf bifurcations (curves) for allometrically determined starvation σ and recovery ρ rates as a function of different mammalian body sizes: $M = P \times 10^2 \text{g}$ (blue) and $M = P \times 10^6 \text{g}$ (green), where P is a random uniform variable in [1, 9]. Points denote realized values of σ and ρ given the drawn values for M .

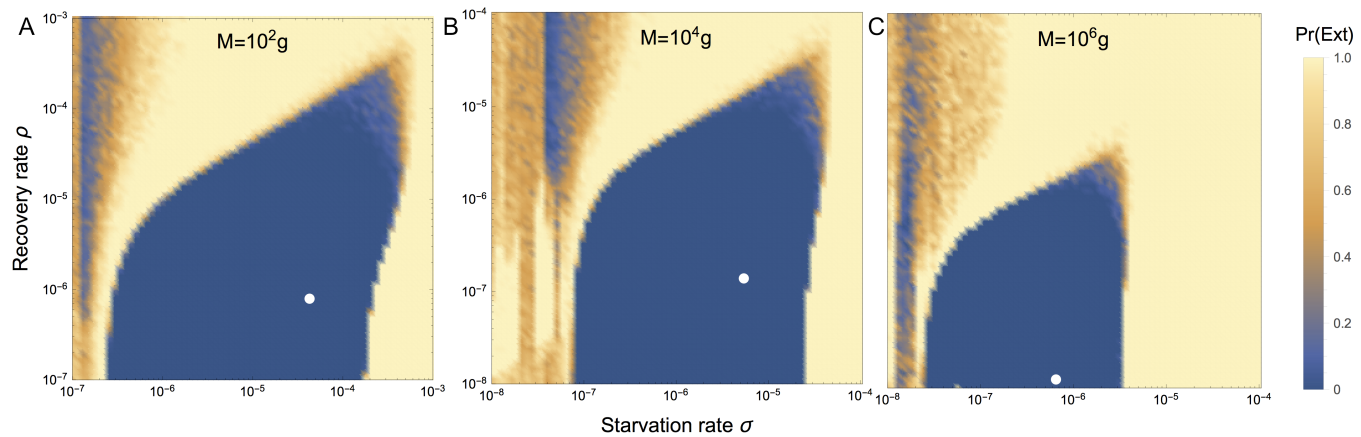


Fig. 5: Probability of extinction for a consumer with (A) $M = 10^2 \text{g}$, (B) $M = 10^4 \text{g}$, and (C) $M = 10^6 \text{g}$ as a function of the starvation rate σ and recovery rate ρ , where the initial density is given as (XF^*, XH^*, R^*) , where X is a random uniform variable in [0, 2]. Note the change in scale for $M = 10^4$ and $M = 10^6 \text{g}$. Extinction is defined as the population trajectory falling below $0.2 \times$ the allometrically constrained steady state. The white points denote the allometrically constrained starvation and recovery rate.

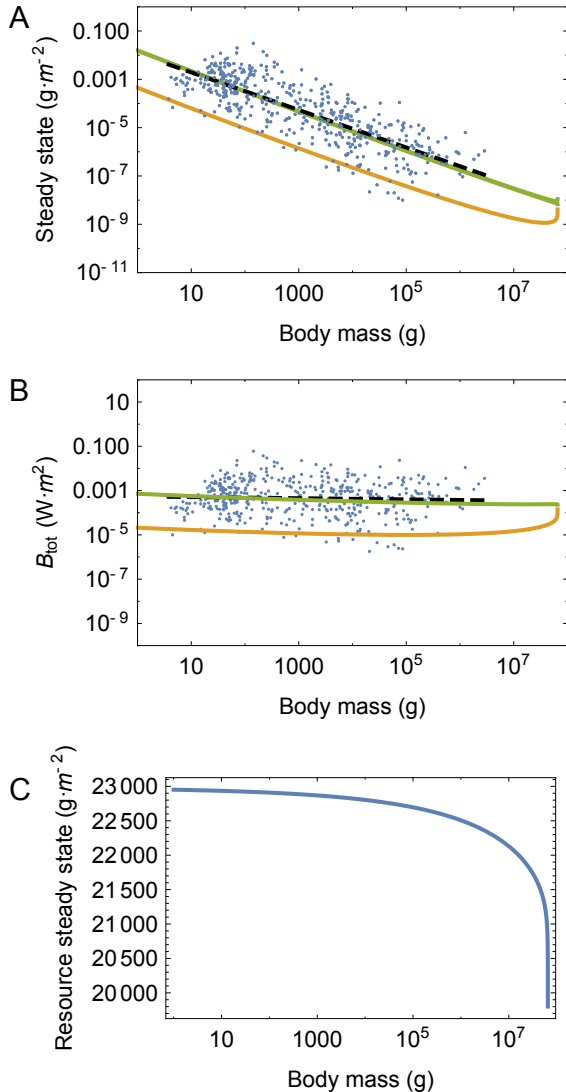


Fig. 6: (A) Consumer steady states F^* (green) and H^* (orange) as a function of body mass. (B) Total energetic use B_{tot} of consumer populations at the steady state as a function of body mass. (C) Resource steady state R^* as a function of consumer body mass. The data are from Damuth (63) and have been converted to total population metabolism using the allometric relationships for metabolic rate (please see SI and Refs. 42, 43, 45).

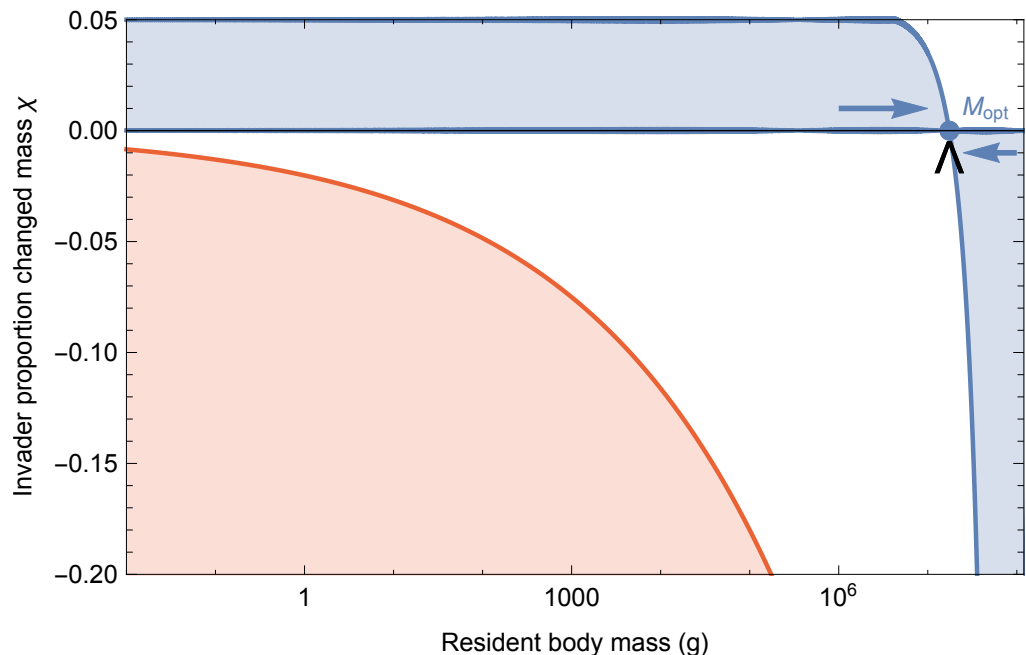


Fig. 7: Invasion feasibility for organisms with a proportional change in mass χ against a population with a resident body mass M . The blue region denotes proportions of modified mass χ resulting in successful invasion. The red region denotes values of χ that result in a mass that is below the starvation threshold and are thus infeasible. Arrows point to the predicted optimal mass from our model $M_{\text{opt}} = 1.748 \times 10^7$, which may serve as an evolutionary attractor for body mass. The black wedge points to the largest body mass known for terrestrial mammals (*Deinotherium* spp.) at 7.74×10^7 g (61).

Supporting Information for “The dynamics of starvation and recovery”

3 Justin D. Yeakel * †‡§, Christopher P. Kempes †‡, and Sidney Redner †¶‡

4 *School of Natural Science, University of California Merced, Merced, CA, †The Santa Fe Institute, Santa Fe, NM, ¶Department of Physics, Boston University, Boston

5 MA, ‡Contributed equally, and §To whom correspondence should be addressed: jdyeakel@gmail.com

6 Submitted to Proceedings of the National Academy of Sciences of the United States of America

7 Mechanisms of Starvation and Recovery

8 Our overall goal is to understand the dynamics of starvation, recovery, reproduction, and resource competition, where
9 our framework partitions starvation and reproduction into two
10 classes of the consumer: a full class that is able to reproduce
11 and a hungry class that experiences mortality at a given rate
12 and is unable to reproduce. For the dynamics of growth, re-
13 production, and resource consumption, past efforts have com-
14 bined the overall metabolic rate as dictated by body size with
15 a growth rate that is dependent on resource abundance and, in
16 turn, dictates resource consumption (see Refs. (1, 2) for a brief
17 review of this perspective). This approach has been used to
18 understand a range of phenomena including a derivation of on-
19 togenetic growth curves from a partitioning of metabolism into
20 maintenance and biosynthesis (e.g. (1, 3–5)) and predictions
21 for the steady-state resource abundance in communities of cells
22 (2). Here we leverage these mechanisms, combined with sev-
23 eral additional concepts, to define our Nutritional State Model
24 (NSM).

We consider the following generalized set of explicit dynam-
ics for starvation, recovery, reproduction, and resource growth
and consumption

$$\begin{aligned}\dot{F}_d &= \lambda(R_d) F_d + \rho(R_d) H_d - \sigma\left(1 - \frac{R_d}{C}\right) F_d, \\ \dot{H}_d &= \sigma\left(1 - \frac{R_d}{C}\right) F_d - \rho(R_d) H_d - \mu H_d, \\ \dot{R}_d &= \alpha R_d \left(1 - \frac{R_d}{C}\right) - \\ &\quad \left[\left(\frac{\rho(R_d)}{Y} + P_H\right) H_d + \left(\frac{\lambda(R_d)}{Y} + P_F\right) F_d\right],\end{aligned}\quad [1]$$

26 where each term has a mechanistic meaning that we detail below
27 (we will denote the dimensional equations with d before intro-
28 ducing the non-dimensional form that is presented in the main
29 text). In this set of equations $\lambda(R_d)$ and $\rho(R_d)$ are the growth
30 and recovery rates as functions of the current resource avail-
31 ability. Typically these can be written as $\lambda(R_d) = \lambda_{max} S(R_d)$
32 or $\lambda(R_d) = \lambda_{max} S(R_d)$ where λ_{max} and ρ_{max} are the maxi-
33 mum growth and recovery rates respectively, which scale with
34 body size as discussed later, and $S(R_d)$ is a saturating func-
35 tion of resources. The saturating function could, for example,
36 be a Michaelis-Menten or Monod function of the form $\frac{R_d}{k+R_d}$,
37 where k is the half-saturation constant. A simplified version
38 of the Michaelis-Menten or Monod functional form, which cap-
39 tures the essential features, is a linear function that saturates
40 to a constant value above a certain abundance of R_d .

41 In the above equations Y represents the yield coefficient
42 (e.g., Refs. 6, 7) which is the quantity of resources required to
43 build a unit of organism (gram of mammal produced per gram
44 of resource consumed) and P is the specific maintenance rate
45 of resource consumption ($\text{g resource} \cdot \text{s}^{-1} \cdot \text{g organism}$). If we
46 pick F_d and H_d to have units of ($\text{g organisms} \cdot \text{m}^{-2}$), then all
47 of the terms of \dot{R}_d , such as $\frac{\rho(R_d)}{Y} H_d$, have units of (g resource

48 $\cdot \text{m}^{-2} \cdot \text{s}^{-1}$) which are the units of net primary productivity
49 (NPP), a natural choice for \dot{R}_d . This choice also gives R_d as (g
50 $\cdot \text{m}^{-2}$) which is also a natural unit and is simply the biomass
51 density. In this system of units $\alpha(\text{s}^{-1})$ is the specific growth
52 rate of R_d , and C is the carrying capacity, or maximum density,
53 of R_d in a particular environment.

Before describing the values of each of these constants, and a general non-dimensionalization of the system of equations, it is important to consider the resource regimes associated with the above equations which lead to a simplification. As discussed above, the resource saturation function should be defined by a linear regime proportional to R_d when $R_d \ll k$, and a constant value for $R_d \gg k$. Thus for hungry individuals, H_d , where $R_d \ll k$, we have that $\rho(R_d) \approx \rho_{max} R_d/k$, and for the full class, F_d , of organisms $\lambda(R_d) \approx \lambda_{max}$, such that the above relationships reduce to

$$\begin{aligned}\dot{F}_d &= \lambda_{max} F_d + \rho_{max} R_d H_d / k - \sigma\left(1 - \frac{R_d}{C}\right) F_d, \\ \dot{H}_d &= \sigma\left(1 - \frac{R_d}{C}\right) F_d - \rho_{max} R_d H_d / k - \mu H_d, \\ \dot{R}_d &= \alpha R_d \left(1 - \frac{R_d}{C}\right) - \\ &\quad \left[\left(\frac{\rho_{max} R_d}{Y_H k} + P_H\right) H_d + \left(\frac{\lambda_{max}}{Y_F} + P_F\right) F_d\right].\end{aligned}\quad [2]$$

We can formally non-dimensionalize this system by choosing the general rescaling of $F = f F_d$, $H = f H_d$, $R = q R_d$, $t = st_d$, in which case our system of equations becomes

$$\begin{aligned}\dot{F} &= \frac{1}{s} \left[\lambda_{max} F + \rho_{max} \frac{R}{qk} H - \sigma\left(1 - \frac{R}{qC}\right) F \right], \\ \dot{H} &= \frac{1}{s} \left[\sigma\left(1 - \frac{R}{qC}\right) F - \rho_{max} \frac{R}{qk} H - \mu H \right], \\ \dot{R} &= \frac{1}{s} \left[\alpha R \left(1 - \frac{R}{qC}\right) - \frac{q}{f} \left[\left(\frac{\rho_{max} R}{Y_H k q} + P_H\right) H + \left(\frac{\lambda_{max}}{Y_F} + P_F\right) F \right] \right]\end{aligned}\quad [3]$$

Reserved for Publication Footnotes

If we make the natural choice of $s = 1$, $q = 1/C$, and individual \cdot g grass $^{-1}$), where B_λ is the lifetime energy use for $f = 1/Y_H k$, then we are left with

$$\begin{aligned}\dot{F} &= \lambda F + \xi \rho R H - \sigma(1-R)F, \\ \dot{H} &= \sigma(1-R)F - \xi \rho R H - \mu H, \\ \dot{R} &= \alpha R(1-R) - (\rho R + \delta)H - \beta F\end{aligned}\quad [4]$$

where we have dropped the subscripts on λ_{max} and ρ_{max} for simplicity, and $\xi = C/k$, $\delta = Y_H k P_H / C$, and $\beta = Y_H k \left(\frac{\lambda_{max}}{Y_F} + P_F \right) / C$. The above equations represent the system of equations presented in the main text.

Parameter Values and Estimates

All of the parameter values employed in our model have either been directly measured in previous studies or can be estimated from combining several previous studies. Below we outline previous measurements and simple estimates of the parameters. Metabolic rate has been generally reported to follow an exponent close to $\eta = 0.75$ (e.g., Refs. 3, 4 and the supplement for Ref. 5). We make this assumption in the current paper, although alternate exponents, which are known to vary between roughly 0.25 and 1.5 for single species (4), could be easily incorporated into our framework, and this variation is effectively handled by the 20% variations that we consider around mean trends. The exponent not only defines several scalings in our framework, but also the value of the metabolic normalization constant, B_0 , given a set of data. For mammals the metabolic normalization constant has been reported to vary between 0.018 (W g $^{-0.75}$) and 0.047 (W g $^{-0.75}$; Refs. 3, 5, where the former value represents basal metabolic rate and the latter represents the field metabolic rate. We employ the field metabolic rate for our NSM model which is appropriate for active mammals (Table 1).

An important feature of our framework is the starting size, m_0 , of a mammal which adjusts the overall timescales for reproduction. This starting size is known to follow an allometric relationship with adult mass of the form $m_0 = n_0 M^\nu$ where estimates for the exponent range between 0.71 and 0.94 (see Ref. 8 for a review). We use $m_0 = 0.097 M^{0.92}$ (9) which encompasses the widest range of body sizes (8).

The energy to synthesize a unit of biomass, E_m , has been reported to vary between 1800 to 9500 (J g $^{-1}$) (e.g. Refs. 3–5) in mammals with a mean value across many taxonomic groups of 5,774 (J g $^{-1}$) (4). The unit energy available during starvation, E' , could range between 7000 (J g $^{-1}$), the return of the total energy stored during ontogeny (5) to a biochemical upper bound of $E' = 36,000$ (J g $^{-1}$) for the energetics of palmitate (5, 10). For our calculations we use the measured value for bulk tissues of 7000 which assumes that the energy stored during ontogeny is returned during starvation (5).

For the scaling of body composition it has been shown that fat mass follows $M_{fat} = f_0 M^\gamma$, with measured relationships following $0.018 M^{1.25}$ (11), $0.02 M^{1.19}$ (12), and $0.026 M^{1.14}$ (13). We use the values from (12) which falls in the middle of this range. Similarly, the muscle mass follows $M_{musc} = u_0 M^\zeta$ with $u_0 = 0.383$ and $\zeta = 1.00$ (13).

Typically the value of $\xi = C/k$ should roughly be 2. The value of ρ , λ , σ , and μ are all simple rates (note that we have not rescaled time in our non-dimensionalization) as defined in the maintext. Given that our model considers transitions over entire stages of ontogeny or nutritional states, the value of Y must represent yields integrated over entire life stages. Given an energy density of $E_d = 18200$ (J g $^{-1}$) for grass (14) the maintenance value is given by $P_F = B_0 M^{3/4} / M E_d$, and the yield for a full organism will be given by $Y_F = M E_d / B_\lambda$ (g

$$B_\lambda = \int_0^{t_\lambda} B_0 m(t)^\eta dt. \quad [5]$$

Similarly, the maintenance for hungry individuals is $P_H = B_0(\epsilon_\sigma M)^{3/4} / (\epsilon_\sigma M) E_d$, and the yield for hungry individuals (representing the cost on resources to return to the full state) is given by $Y_H = M E_d / B_\rho$ where

$$B_\rho = \int_{\tau(\epsilon_\sigma \epsilon_\lambda)}^{t_\lambda} B_0 m(t)^\eta dt. \quad [6]$$

Taken together, these relationships allow us to calculate ρ , δ , and β .

Finally, the value of α can be roughly estimated by the NPP divided by the corresponding biomass densities. From the data in Ref. 15 we estimate the value of α to range between 2.81×10^{-10} (s $^{-1}$) and 2.19×10^{-8} (s $^{-1}$) globally. It should be noted that the value of α sets the overall scale of the F^* and H^* steady states along with the B_{tot} for each type, and as such, we use α as our fit parameter to match these steady states with the data from Damuth (16). We find that the best fit is $\alpha = 9.45 \times 10^{-9}$ (s $^{-1}$) which compares well with the calculated range above. However, two points are important to note here: first, our framework predicts the overall scaling of F^* and H^* independently of α and this correctly matches data, and second, both the asymptotic behavior and slope of F^* and H^* are independent of α , such that our prediction of the maximum mammal size does not depend on α .

Table 1: Parameter values for mammals

Parameter	Value	References
η	3/4	(e.g. (3–5))
E_m	5774 (J gram $^{-1}$)	(3–5)
E'_m	7000	(5, 10)
B_0	0.047 (W g $^{-0.75}$)	(5)
γ	1.19	(12)
f_0	0.02	(12)
ζ	1.00	(13)
u_0	0.38	(13)

Rate equations for invaders with modified body mass We allow an invading subset of the resident population with mass M to have an altered mass $M' = M(1 + \chi)$ where χ varies between $\chi_{min} < 0$ and $\chi_{max} > 0$, where $\chi < 0$ denotes a leaner invader and $\chi > 0$ denotes an invader with additional reserves of body fat. Importantly, we assume that the invading and resident individuals have the same proportion of non-fat tissues. For the allowable values of χ the adjusted mass should exceed the amount of body fat, $1 + \chi > \epsilon_\sigma$, and the adjusted time to reproduce must be positive, which given our solution for $\tau(\epsilon)$ (see main text), implies that $1 - \epsilon_\lambda^{1-\eta} (1 + \chi)^{1-\eta} > 0$. Together these conditions imply that $\chi \in (-f_0 M^{\gamma-1}, 1/\epsilon_\lambda - 1)$ where the upper bound approximately equals 0.05.

Although the starved state of invading organisms remains unchanged, the rate of starvation from the modified full state to the starved state, the rate of recovery from the starved state to the modified full state, and the maintenance rates of both, will be different, such that $\sigma' = \sigma(M')$, $\rho' = \rho(M')$, $\beta' = \beta(M')$, $\delta' = \delta(M')$. Rates of starvation and recovery for the invading population are easily derived by adjusting the starting or ending state before and after starvation and recovery, leading to the following timescales:

$$t_{\sigma'} = -\frac{M^{1-\eta}}{a'} \ln \left(\frac{\epsilon_\sigma}{\chi + 1} \right),$$

$$t_{\rho'} = \ln \left(\frac{1 - (\epsilon_\lambda \epsilon_\sigma)^{1/4}}{1 - (\epsilon_\lambda (\chi + 1))^{1/4}} \right) \frac{M^{1-\eta}}{a' (1 - \eta)}.$$

The maintenance rates for the invading population require more careful consideration. First, we must recalculate the yields Y , as they must now be integrated over life stages that have also been slightly modified by the addition or subtraction of body fat reserves. Given an energy density of $E_d = 18200 \text{ (J g}^{-1}\text{)}$ for grass (14) the maintenance value of the invading population is given by $P_F = B_0(1 + \chi)M^{3/4}/(1 + \chi)ME_d$, and the yield for a full organism will be given by $Y_F = (1 + \chi)ME_d/B'_\lambda$ (g individual \cdot g grass $^{-1}$) where B'_λ is the lifetime energy use for the invading population reaching maturity given by

$$B'_\lambda = \int_0^{t_{\lambda'}} B_0 m(t)^\eta dt.$$

where

$$t_{\lambda'} = \frac{M^{1-\eta}}{a(1 - \eta)} \ln \left(\frac{1 - (m_0/M)^{1-\eta}}{1 - (\epsilon_\lambda(1 + \chi))^{1-\eta}} \right).$$

Note that we do not use this timescale to determine the reproductive rate of the invading consumer—which is assumed to remain the same as the resident population—but only to calculate the lifetime energy use. Similarly, the maintenance for hungry individuals $P'_H = B_0(\epsilon_\sigma(1 + \chi)M)^{3/4}/(\epsilon_\sigma(1 + \chi)M)E_d$ and the yield for hungry individuals (representing the cost on resources to return to the full state) is given by $Y'_H = (1 + \chi)ME_d/B'_\rho$ where

$$B'_\rho = \int_{\tau(\epsilon_\sigma \epsilon_\lambda)}^{t_{\lambda'}} B_0 m(t)^\eta dt.$$

Finally, we can calculate the maintenance of the invaders as

$$\delta' = P'_H Y'_H / \xi$$

$$\beta' = \left(\frac{\lambda_{\max}}{Y'_F} + P'_F \right) Y'_H / \xi.$$

To determine whether or not the invader or resident population has an advantage, we compute $R^*(M)$ and $R^*(M' = M(1 + \chi))$ for values of $\chi \in (-f_0 M^{\gamma-1}, 1/\epsilon_\lambda - 1)$, and the invading population is assumed to have an advantage over the resident population if $R^*(M') < R^*(M)$.

References

- [7] 181 Kempes CP, Dutkiewicz S, Follows MJ (2012) Growth, metabolic partitioning, and the size of microorganisms. *PNAS* 109:495–500.
- [8] 182 Kempes CP, Okegbé C, Mears-Clarke Z, Follows MJ, Di- 183 etrich LE (2014) Morphological optimization for access 184 to dual oxidants in biofilms. *Proceedings of the National 185 Academy of Sciences* 111:208–213.
- [9] 186 West GB, Brown JH, Enquist BJ (2001) A general model 187 for ontogenetic growth. *Nature* 413:628–631.
- [10] 188 Moses ME, et al. (2008) Revisiting a model of ontogenetic 189 growth: Estimating model parameters from theory and 190 data. <http://dx.doi.org.proxy.lib.sfu.ca/10.1086/679735> 191 171:632–645.
- [11] 192 Hou C, et al. (2008) Energy uptake and allocation during 193 ontogeny. *Science* 322:736–739.
- [12] 194 Pirt S (1965) The maintenance energy of bacteria in growing 195 cultures. *Proceedings of the Royal Society of London B: Biological Sciences* 163:224–231.
- [13] 196 Heijnen J, Roels J (1981) A macroscopic model describing 197 yield and maintenance relationships in aerobic fermentation 198 processes. *Biotechnology and Bioengineering* 23:739–763.
- [14] 199 Peters RH (1986) *The Ecological Implications of Body Size* 200 (Cambridge University Press, Cambridge) Vol. 2.
- [15] 201 Blueweiss L, et al. (1978) Relationships between body size 202 and some life history parameters. *Oecologia* 37:257–272.
- [16] 203 Stryer L (1995) *Biochemistry, Fourth Edition* (W.H. Freeman and Company, New York), pp 608–611.
- [17] 204 Dunbrack RL, Ramsay MA (1993) The Allometry of Mammalian Adaptations to Seasonal Environments: A Critique of the Fasting Endurance Hypothesis. *Oikos* 66:336–342.
- [18] 205 Lindstedt SL, Boyce MS (1985) Seasonality, Fasting Endurance, and Body Size in Mammals. *Am. Nat.* 125:873–878.
- [19] 214 Lindstedt SL, Schaeffer PJ (2002) Use of allometry in predicting anatomical and physiological parameters of mammals. *Lab. Anim.* 36:1–19.
- [20] 215 Estermann BL, Wettstein HR, Sutter F, Kreuzer M (2001) 216 Nutrient and energy conversion of grass-fed dairy and suckler 217 beef cattle kept indoors and on high altitude pasture. *Animal Research* 50:477–493.
- [21] 218 Michaletz ST, Cheng D, Kerkhoff AJ, Enquist BJ (2014) 219 Convergence of terrestrial plant production across global 220 climate gradients. *Nature* 512:39–43.
- [22] 221 Damuth J (1987) Interspecific allometry of population density 222 in mammals and other animals: the independence of body mass and population energy-use. *Biological Journal of the Linnean Society* 31:193–246.